Motion of 1/3111 dislocations on Σ3 {112} twin boundaries in nanotwinned copper

N. Lu, K. Du, L. Lu, and H. Q. Ye

Articles you may be interested in

Dislocation structures of Σ 3 {112} twin boundaries in face centered cubic metals
Appl. Phys. Lett. **95**, 021908 (2009); 10.1063/1.3176979

Atomic-scale in situ observation of lattice dislocations passing through twin boundaries
Appl. Phys. Lett. **94**, 021909 (2009); 10.1063/1.3072801

Structure and migration of (112) step on (111) twin boundaries in nanocrystalline copper
J. Appl. Phys. **104**, 113717 (2008); 10.1063/1.3035944

Dynamical dislocation emission processes from twin boundaries
Appl. Phys. Lett. **93**, 041906 (2008); 10.1063/1.2965637

Deformation twinning in nanocrystalline copper at room temperature and low strain rate
Appl. Phys. Lett. **84**, 592 (2004); 10.1063/1.1644051

2014 Special Topics

PEROVSKITES

2D MATERIALS

MESOPOROUS MATERIALS

BIOMATERIALS/ BIOELECTRONICS

METAL-ORGANIC FRAMEWORK MATERIALS

AIP | APL Materials

Submit Today!

Motion of 1/3⟨111⟩ dislocations on Σ3 {112} twin boundaries in nanotwinned copper

N. Lu,[1,2] K. Du,[1,2,a] L. Lu,[1] and H. Q. Ye[1]

[1]*Shenyang National Laboratory for Materials Science, Institute of Metal Research, Chinese Academy of Sciences, Shenyang 110016, China*
[2]*Beijing National Center for Electron Microscopy, Tsinghua University, Beijing 100084, China*

The atomic structure of Σ3 {112} ITBs in nanotwinned Cu is investigated by using aberration-corrected high resolution transmission electron microscopy (HRTEM) and *in situ* HRTEM observations. The Σ3 {112} ITBs are consisted of periodically repeated three partial dislocations. The *in situ* HRTEM results show that 1/3[111] partial dislocation moves on the Σ3 {112} incoherent twin boundary (ITB), which was accompanied by a migration of the ITB. A dislocation reaction mechanism is proposed for the motion of 1/3[111] Frank partial dislocation, in which the 1/3[111] partial dislocation exchanges its position with twin boundary dislocations in sequence. In this way, the 1/3[111] dislocation can move on the incoherent twin boundary in metals with low stacking fault energy. Meanwhile, the ITB will migrate in its normal direction accordingly. These results provide insight into the reaction mechanism of 1/3[111] dislocations and ITBs and the associated migration of ITBs. © 2014 AIP Publishing LLC. [http://dx.doi.org/10.1063/1.4861868]

I. INTRODUCTION

Copper with a high density of nanotwins has attracted considerable interest over the past years attributed to its excellent mechanical properties including high strength and ductility.[1–3] Recent experimental results suggest that such excellent mechanical properties depend to a large extent on the interaction between lattice dislocations and twin boundaries (TBs).[1,4,5] Twin boundaries with {111} and {112} planes in fcc metals are often designated as coherent twin boundaries (CTBs) and incoherent twin boundaries (ITB), respectively.[6] The structure and energy of the twin boundaries have been extensively investigated by theoretical simulation and experiments.[7–13] CTBs, serving as strong barriers to dislocation movement and as dislocation emission sources, play a significant role in strengthening and maintaining the ductility.[14–16] The migration of CTBs is reported via the gliding of Shockley partials on them, which is promoted by imposed shear stress.[17] Twin boundaries might also act as non-regenerative dislocation sources that would induce the migration of CTBs during plastic deformation.[18] Meanwhile, incoherent segments on CTBs or ITBs play an important role in the detwinning mechanism and mechanical behavior of nanotwinned materials.[4,19] ITBs are usually described as a set of Shockley partial dislocations on every {111} plane with a periodically repeated three-layer sequence.[20] Experimental results for metals with low stacking fault energy (SFE) (such as Cu and Ag) show that the detwinning process or migration of ITBs can be accomplished via the collective glide of those Shockley partial dislocations.[19,21] Xu *et al.*[22] observed that the motion of [11$\bar{2}$] twin steps in (111)/(11$\bar{2}$)/(111) junctions dominates the migration of ITBs. Brown and Ghoniem[23] proposed that the moving of

CTB/ITB junctions is carried out by kink-like motion of neighboring atomic columns. Medlin *et al.*[24] revealed independent glide and climb of the 1/3[111] dislocations on ITB and CTB, respectively, in aluminum with high SFE. The climb of 1/3[111] dislocations is associated with the moving of ITBs. Molecular statics and dynamics calculations obtained different ITB structures for metals with varied stacking fault energies, whereas the ITBs were considered to be dissociated into two phase boundaries bounding a hexagonal 9R phase.[25] For low SFE metals such as Cu, under shear stress one of the phase boundaries migrates parallel to the ITB normal vector, referred to phase-boundary-migration mechanism. For high SFE metals such as Al, ITBs experience a coupled motion through the glide of interface disconnections with a Burgers vector of 2a/3[111] and a step component of a/6[11$\bar{2}$], referred to as interface-disconnection-glide mechanism. Therefore, further analysis is desired at the atomic level for the migration of Σ3 {112} ITBs in fcc metals.

In this paper, we have investigated nanotwinned Cu by *in situ* high-resolution transmission electron microscopy (HRTEM) technique. 1/3[111] Frank partial dislocation was observed moving on the Σ3 {112} incoherent twin boundary. Accordingly, the incoherent twin boundary migrated along the direction normal to the ITB plane. A dislocation exchange mechanism was proposed and it successfully explains the moving process of the 1/3[111] partial dislocation. This moveable grain boundary dislocation might offer a route for the migration of Σ3 {112} ITBs, especially for metals with low stacking fault energy.

II. EXPERIMENTAL

An equiax-grained Cu foil was used in the experiment with the thickness of 70 μm.[26,27] Transmission electron microscopy (TEM) specimens with 3 mm diameter were cut

a)Email address: kuidu@imr.ac.cn.

from the foil and thinned by double-jet electropolishing in solution of 25% phosphoric acid, 25% ethanol, and 50% distilled water at 263 K. The atomic structure of ITB was resolved with an aberration-corrected transmission electron microscope (Titan 80–300) operating at 300 kV with a spatial resolution of 0.08 nm. *In situ* tensile experiment was conducted using a Gatan 654 single-tilt straining holder in a FEI Tecnai F30 TEM operating at 300 kV with a spatial resolution of 0.20 nm. Detailed *in situ* TEM straining procedures and sample preparation are described in Ref. 28. Time-resolved high resolution transmission electron microscopy (HRTEM) images were recorded as digital video with 10 fps, corresponding to a time resolution of 0.1 s for the *in situ* observation.

III. RESULTS

The Cu sample has high density of growth twins (see Figs. 1(a) and 1(b)), which facilitate the investigation of twin boundary effects on plastic deformation of nanotwinned metals. Fig. 1(c) shows the microstructure of two typical twin boundaries, i.e., Σ3 {111} coherent twin boundary (CTB) and Σ3 {112} incoherent twin boundary (ITB). (A discussion on the image contrast of the ITB is presented in Ref. 28).

A. Atomic structure of the ITB

The atomic structure of Σ3 {112} ITBs in nanotwinned Cu is clearly illustrated by the aberration-corrected HRTEM imaging (Fig. 2(a)), which effectively eliminates delocalization effects from HRTEM imaging.[29] The ITB structure can be described as a set of Shockley partial dislocations on every {111} planes with a periodically repeated three-layer sequence, similar to the generally reported ITB structures for fcc metals with different SFE such as Cu and Al by experimental investigations and MD simulations.[20,25] The nature of these periodic three-layer partial dislocations was determined as two 30° Shockley partials ($A\delta$ and $B\delta$) and a 90° Shockley partial ($C\delta$), as shown in Fig. 2(b).

The ITBs can dissociate into two phase boundaries with a dissociation region scales inversely with the SFE.[25] For instance, one phase boundary comprised of 30° Shockley partials and the other comprised of 90° Shockley partials. We have measured their dissociation extent by quantitative image analysis with a lattice distortion analysis program (LADIA[30]) on Fig. 2(a). The angle θ between two basic

vectors u and v is employed to define the crystal lattices across the ITB, and the distribution of angle θ is shown in Fig. 2(c), correspondingly. Line profiles were extracted from the analysis results for three adjacent (111) planes in one periodic set of Shockley dislocations, as shown in Fig. 2(d). Whereas the angle θ in the left half crystal is about 70.5°, the one in the right half crystal is about 54.75°. The line profiles show that the extent of dissociation in Cu is about 0.3–0.4 nm, which is much smaller than the simulation results (0.8 nm) but comparable to that of Al (0.3 nm).[25] The projected spacing between two adjacent (112) atomic planes is a/4[112] (0.22 nm) along the [110] projection, therefore, the width of ITB just corresponds to about two atomic planes.

B. Dynamic process of the 1/3[111] partial dislocation on the ITB

Aberration-corrected HRTEM (Fig. 2(a)) and conventional HRTEM (Fig. 3(a)) images both show the obvious symmetric orientation relationship across the ITBs. The change of lattice orientation across CTBs and the ITB in Fig. 3(a) is presented in Ref. 28 for clarity. A box marks a dislocation on the ITB. Noteworthy, this dislocation is not a part of the ITB. A magnified image of the dislocation is given in Fig. 3(b), which shows its Burgers vector of 1/3[111].

Time resolved HRTEM images (Fig. 4) reveal the dynamic process of the 1/3[111] partial dislocation moving on the ITB under external stress (details see movie 1 (Ref. 28)). To clearly show the lattice distortion around the 1/3[111] partial, fast-Fourier-transformation (FFT) analysis has been performed on the HRTEM images. Compared with the HRTEM images (Figs. 4(a)–4(d)), the corresponding FFT images with plane fringes (Figs. 4(e)–4(h)) show much clearly the location of the 1/3[111] partial and the spread of dislocation core on the ITB. In Figs. 4(a) and 4(e), the 1/3[111] partial located at the lower end of the ITB. During the continuous observation, the 1/3[111] partial moved upward on the ITB, as shown in Figs. 4(b) and 4(f), till the upper end of the ITB in Figs. 4(c) and 4(g). After the dislocation reached the upper end, a Shockley partial dislocation was emitted from the location of the 1/3[111] partial, leaving behind a stacking fault (see Figs. 4(d) and 4(h)).

The positions of the 1/3[111] partial before and after the moving process are shown in Fig. 5(a) (t = 0 s) and Fig. 5(b)
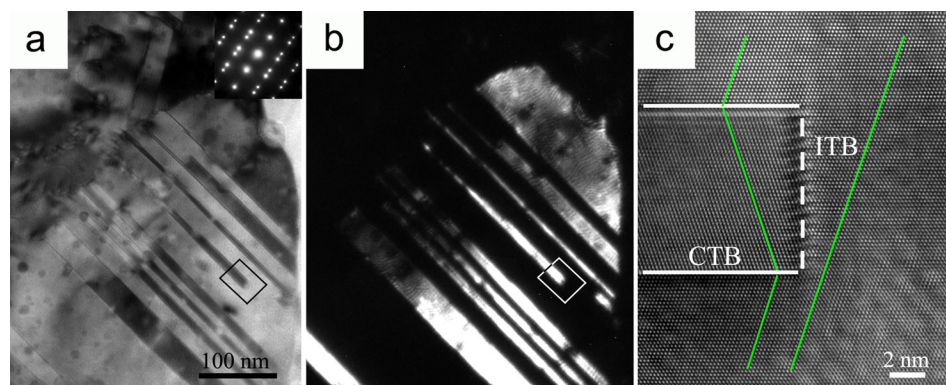

FIG. 1. (a) A bright field TEM image of nanotwinned copper. Inset is a selected-area diffraction pattern obtained from the observed area. (b) The corresponding dark field image. (c) A HRTEM image of the area marked by the box in (a) and (b), showing two types of twin boundaries, coherent twin boundaries (CTBs) and an incoherent twin boundary (ITB). The lattice orientations are indicated by green lines. The CTBs and ITB are indicated by solid and dashed white lines, respectively.
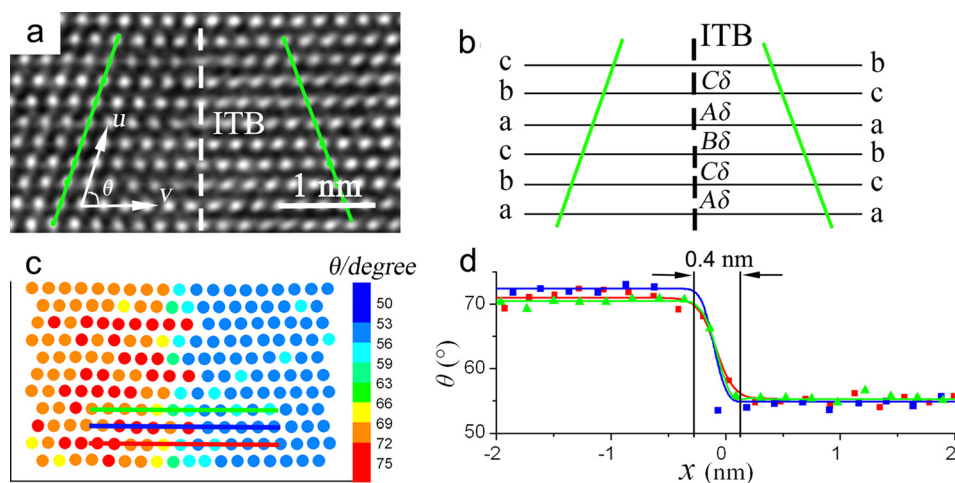
FIG. 2. (a) Aberration-corrected HRTEM image of an ITB. The lattice orientations are indicated by green lines, which show clearly a symmetric orientation relationship between two half crystals. The ITB is indicated by a dashed white line. (b) Schematic illustration of the periodic three-layer partial dislocations in the ITB of (a) as two 30° Shockley partials ($A\delta$ and $B\delta$) and a 90° Shockley partial ($C\delta$). (c) The distribution of the angle θ between two basic vectors u and v, as denoted in (a), measured by the lattice distortion analysis program from the aberration-corrected HRTEM image. (d) Line profiles of the angle θ variation across the ITB along three adjacent (111) planes. The three (111) planes are denoted by three lines in red, blue, and green, respectively, in (c).
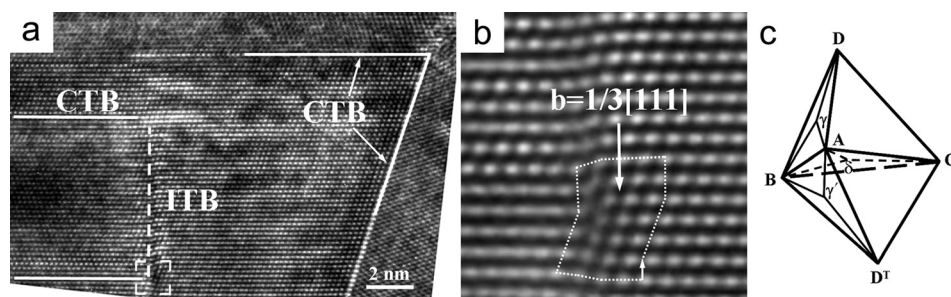

FIG. 3. (a) An HRTEM image of an ITB at another sample area different from that of Fig. 1. The change of lattice orientation across CTBs and ITB is presented in Supplementary Chap. 3. A dislocation (marked by the circle) is at the ITB. (b) A magnified image of the dislocation in (a). The Burgers circuit shows that the Burgers vector of this dislocation is 1/3[111]. (c) A double Thompson tetrahedron.
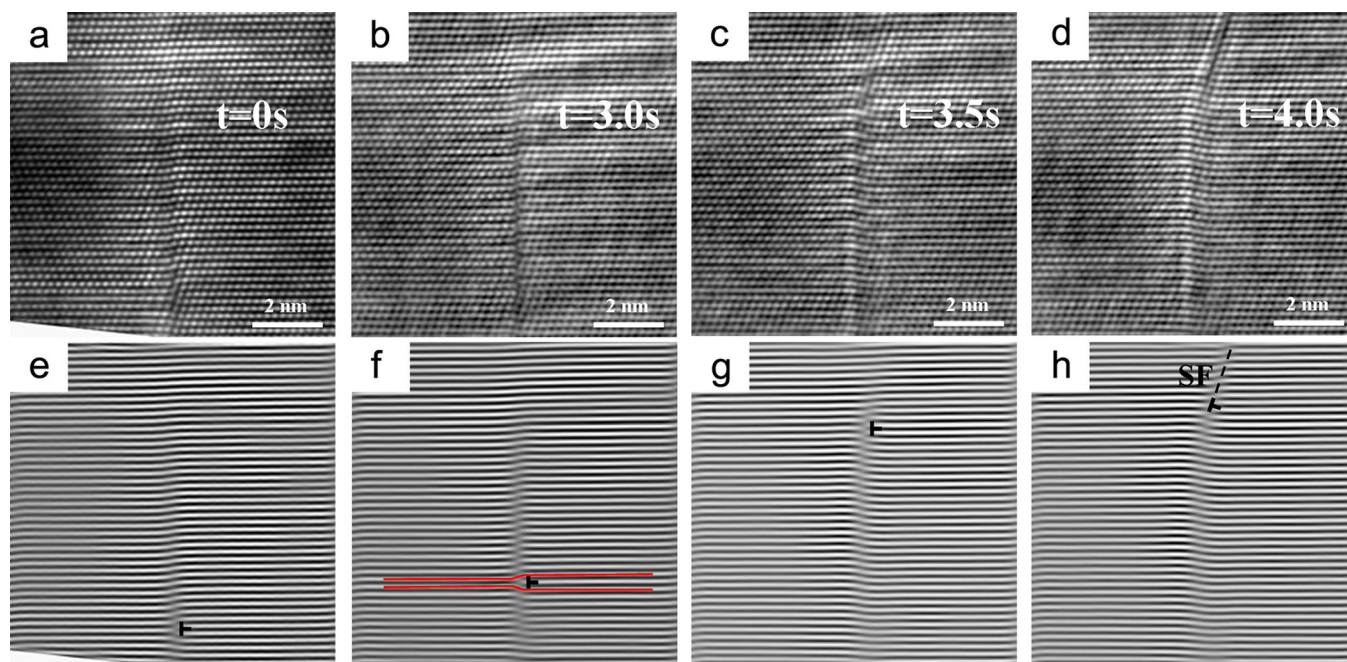

FIG. 4. (a)-(d) A series of *in situ* HRTEM images, showing the motion of 1/3[111] partial dislocation on ITB. (e)-(h) Corresponding fast-Fourier-transformed (FFT) images with (111) plane fringes clearly show locations of the 1/3[111] partial. The dislocation core of the 1/3[111] partial in (f) is marked by red lines (Multimedia view). [URL: http://dx.doi.org/10.1063/1.4861868.1][28]
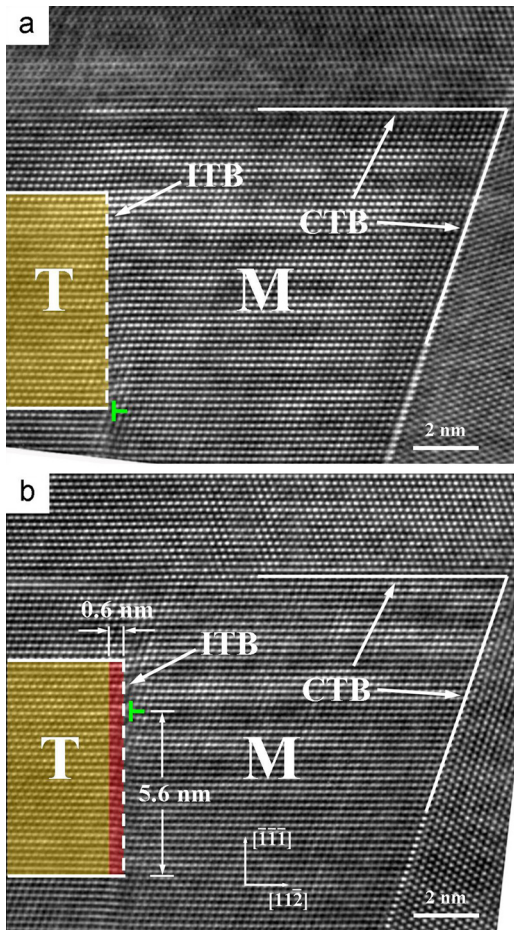
FIG. 5. (a)-(b) HRTEM images show positions of the ITB (marked by dashed line) and the 1/3[111] partial before (t = 0 s) and after (t = 3.5 s) the moving process, respectively. The dislocation position is denoted by the green symbol of dislocation. Two reference lines, which are two CTBs, are indicated by the white arrows. The initial area of the twin lamella is marked with yellow; the area passed by the migrating ITB is marked with red. T and M represent the twin and matrix regions, respectively.

(t = 3.5 s), respectively. It reveals that the 1/3[111] partial dislocation moves across 5.6 nm along $[\bar{1}\bar{1}\bar{1}]$ direction and about 0.6 nm along $[11\bar{2}]$ direction. Locations of the 1/3[111] partial are determined from two reference lines, which are a coherent twin boundary on the right and another coherent twin boundary at 45 (111) layers above the lower end of the ITB. These two reference lines remain their original positions during the whole process. Meanwhile, the ITB moves to the right with 0.6 nm, which is indicated by red color in Fig. 5(b). The location of ITBs is determined by the relative shift of the (111) planes.[28]

IV. THEORETICAL ANALYSIS AND DISCUSSION

The motion of 1/3[111] partial on ITBs is in contrast to the non-glissile feature of 1/3[111] Frank dislocation in a perfect crystal.[31] In this section, a dislocation-exchange mechanism is proposed for the moving process of the 1/3[111] partial dislocation on the ITB, where the 1/3[111] partial exchanges its position with the ITB partial dislocations in sequence. Additionally, the exact moving direction of the 1/3[111] partial is determined from the experimental

observation and compared with the gliding plane predicted from the dislocation-exchange model. Then, the shear stress needed for the dislocation reactions is estimated for the exchange of dislocation positions based on this model. At last, we explain the emission of a 30° Shockley partial dislocation from the location of 1/3[111] partial at the upper end of the ITB.

A. Gliding model of the 1/3[111] partial on the ITB

Fig. 3(c) shows a double Thompson tetrahedron,[32] which demonstrates the geometric relationship of crystal lattices at two sides of the ITB. In this work, the viewing direction is along AB ($1/2[\bar{1}10]$) for HRTEM investigation. Accordingly, the set of two 30° Shockley partials and a 90° Shockley partial in the ITB are denoted as $A\delta$, $B\delta$, and $C\delta$, respectively. The 1/3[111] dislocation is denoted as $D\delta$ in the Thompson tetrahedron. Since a full dislocation (e.g., DA) in the matrix would easily react with an adjacent ITB partial (e.g., $A\delta$) and form a 1/3[111] partial dislocation ($D\delta$), a 1/3[111] partial dislocation is more stable on the ITB than a full dislocation.
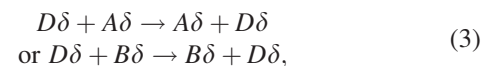
As shown in Fig. 6, the gliding process of 1/3[111] partial can be considered as a specific set of dislocation reactions between the 1/3[111] partial and ITB partial dislocations. Fig. 6(a) shows that the 1/3[111] partial $D\delta$ locates at the lower end of the ITB (defined as 0th plane of the left half-crystal relative to the ITB, the (111) plane above termed as 1st plane, correspondingly). Driven by applied stress, the 1/3[111] partial dissociates into a partial dislocation $A\delta$ and a full dislocation DA on the 0th plane of the left half-crystal (see Fig. 6(b)), i.e.,

$$D\delta \rightarrow A\delta + DA$$
$$\text{or } D\delta \rightarrow B\delta + DB. \tag{1}$$
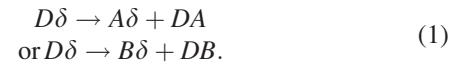
Subsequently, the full dislocation DA glides up on the $(11\bar{1})$ (plane ABD in the Thompson tetrahedron) to the above (111) plane (1st plane of the left half-crystal) and reacts there with the partial $A\delta$ to form a new 1/3[111] partial $D\delta$ (Figs. 6(c) and 6(d)):

$$DA + A\delta \rightarrow D\delta$$
$$\text{or } DB + B\delta \rightarrow D\delta. \tag{2}$$
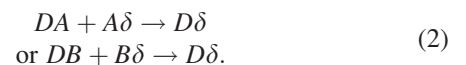
The overall reaction is

$$D\delta + A\delta \rightarrow A\delta + D\delta$$
$$\text{or } D\delta + B\delta \rightarrow B\delta + D\delta, \tag{3}$$

which is equivalent to the dislocations $D\delta$ and $A\delta$ exchange their positions. After that, 1/3[111] partial $D\delta$ can repeat the above dislocation reactions and simply exchange its position with the next partial dislocation $B\delta$. As a result, the 1/3[111] partial dislocation go further up to the next (111) plane (see Fig. 6(e)).

Different from the two 30° Shockley dislocations $A\delta$ and $B\delta$, for the 90° Shockley dislocation $C\delta$, the 1/3[111] partial $D\delta$ needs to dissociate into two partial dislocations, i.e., $C\delta$ on the 2nd (111) plane and $A\delta$ on the 3rd (111) plane
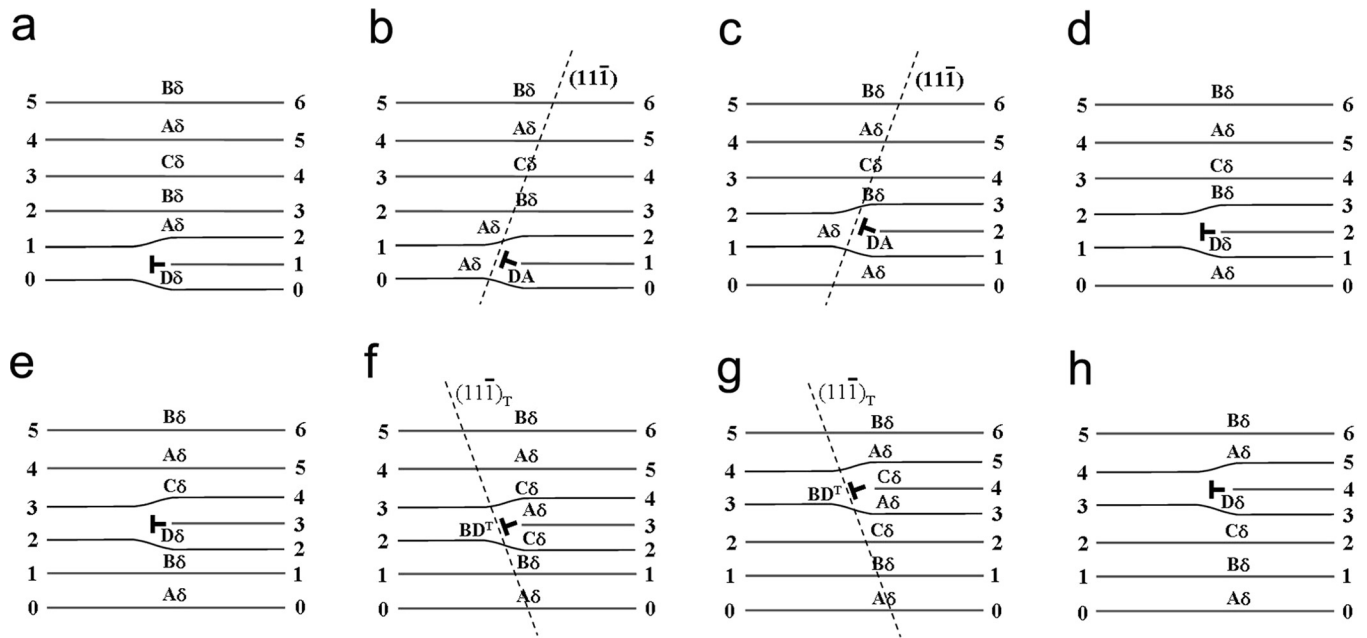
FIG. 6. Schematic illustrates of the gliding process of a 1/3[111] partial on the Σ3 {112} ITB. The lowest (111) plane is defined as 0th plane of the left and right half-crystal, respectively; while the above (111) planes are termed as 1st, 2nd,… 6th plane, correspondingly. (a) The 1/3[111] partial, $D\delta$, locates at the lower end of the ITB. (b)-(d) After the dissociation of $D\delta$ into DA and $A\delta$, DA glides up on $(11\bar{1})$ by one atomic plane and reacts there with the ITB partial $A\delta$ (on the 1st plane of the left half-crystal) to form a new 1/3[111] partial $D\delta$. (e) Similarly, $D\delta$ and $B\delta$ exchange their positions with the above process. (f) $D\delta$ dissociates into two partial dislocations, i.e., $C\delta$ on the 2nd (111) plane and $A\delta$ on the 3rd (111) plane of the right half-crystal, and a full dislocation BD^T on the 2nd (111) plane of the left half-crystal. (g)–(h) BD^T glides up on $(11\bar{1})_T$ by one atomic plane and reacts with two partials there, i.e., $A\delta$ on the 3rd (111) plane and $C\delta$ on the 4th (111) plane of the right half-crystal, to form a new 1/3[111] partial $D\delta$.

of the right half-crystal, and a full dislocation BD^T on the 2nd (111) plane of the left half-crystal (see Fig. 6(f)) as

$$D\delta \rightarrow C\delta + A\delta + BD^T. \tag{4}$$

Subsequently, the full dislocation BD^T glides up on $(11\bar{1})_T$ (plane ABD^T in the Thompson tetrahedron) to the 3rd (111) plane of the left half-crystal and reacts with two partials there, i.e. $A\delta$ on the 3rd (111) plane of the right half-crystal and $C\delta$ on the 4th (111) plane of the right half-crystal, and consequently form a new 1/3[111] partial $D\delta$ (see Figs. 6(g) and 6(h))

$$BD^T + A\delta + C\delta \rightarrow D\delta. \tag{5}$$

The overall reaction

$$D\delta + C\delta \rightarrow C\delta + D\delta \tag{6}$$

results the exchange of positions between the Frank dislocation $D\delta$ and the 90° Shockley dislocation $C\delta$. Although the exchange of dislocation positions is described as a set of reactions, the overall process also corresponds to an atomic shuffling at two atomic layers. The detailed exchange reaction is very fast so that it is not observable in the current *in situ* study. In this regard, the ultrafast electron microscopy may provide interesting results when time resolution and atomic resolution are both realized there in the future.[33]

In this way, the 1/3[111] partial can carry on the above dislocation reactions and exchange positions with the ITB partials as described in Eqs. (1)–(6) and illustrated in Figs. 6(a)–6(h), causing the motion of 1/3[111] partial on the ITB.

Although the source of the 1/3[111] partial has not been investigated in the present study. One mechanism is that it might be generated as an interaction product between the lattice dislocation 1/2[110] and the Σ3 {112} ITBs (e.g., 1/6[-1-1 2]). For example, Medlin *et al.*[24] reported that full dislocations could interact with Σ3 {112} ITBs and form 1/3 partial dislocations in Al crystal.

B. The exact moving plane of the 1/3[111] partial

According to the formula $\boldsymbol{l} = \xi \times \boldsymbol{b}$, where $\xi = AB$ $(1/2[\bar{1}10])$ is the sense of the 1/3[111] partial dislocation and $\boldsymbol{b} = 1/3[111]$ is the Burgers vector, the gliding plane $\boldsymbol{l}$ would correspond to $(11\bar{2})$.[31] However, comparing positions of the 1/3[111] partial dislocation during its moving process (at $t = 0\,s$, $3.0\,s$ and $3.5\,s$, respectively), which are summarized and plotted in Fig. 7(a), the three positions lie in a straight line, which would correspond to a moving plane for the 1/3[111] dislocation. An angle $\varphi \approx 7°$ is determined between this moving plane and the ITB plane. Correspondingly, the 1/3[111] partial moves across about 5.6 nm (27 (111) layers) along the $[\bar{1}\bar{1}\bar{1}]$ direction and about 0.6 nm along the $[11\bar{2}]$ direction during the process.

According to the proposed model, after the exchange between the 1/3[111] partial $D\delta$ and the ITB partial dislocations $A\delta$, $B\delta$ and $C\delta$, the 1/3[111] partial will glide up respectively on $(11\bar{1})$, $(11\bar{1})$ (indicated by red arrows) and $(11\bar{1})_T$ (indicated by blue arrow) by each (111) plane, as shown in Fig. 7(b). And it is $1/12[11\bar{2}]a$, $1/12[11\bar{2}]a$, and $-1/12[11\bar{2}]a$ under the projection of [111], respectively. Consequently, the total movement of 1/3[111] partial is
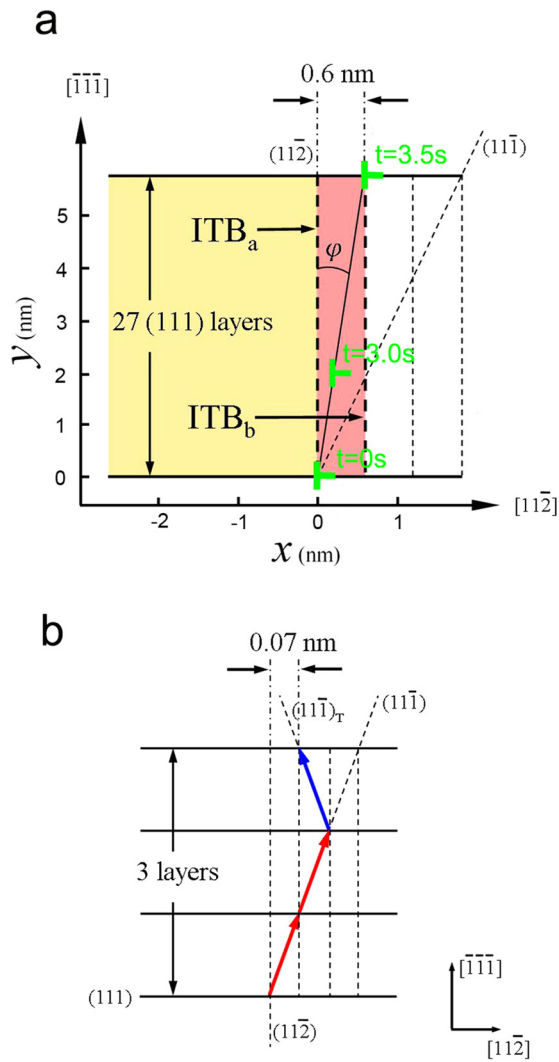
a

b

FIG. 7. (a) Plot of the position of the 1/3[111] partial during its moving process (at t = 0 s, 3.0 s, and 3.5 s), where the dislocation position is denoted by the green symbol of dislocation. An angle $\varphi \approx 7°$ is determined between this moving direction and the ITB plane. Positions of the ITB before (t = 0 s) and after (t = 3.5 s) the migration are indicated by ITB$_a$ and ITB$_b$, respectively. The 1/3[111] partial moves up ~5.6 nm (27 (111) layers) along the $[\bar{1}\bar{1}1]$ direction and right ~0.6 nm along the $[11\bar{2}]$ direction during the process. (b) Schematics of the dislocation motion carried out by the exchange between 1/3[111] partial $D\delta$ and ITB partial dislocations $A\delta$, $B\delta$, and $C\delta$, which are indicated by red, red and blue arrows, respectively.

$1/12[11\bar{2}]a$, 0.07 nm, along $[11\bar{2}]$ direction after move across three (111) layers. When the 1/3[111] partial moves across 27 layers (111) plane, it will move about 0.63 nm along the $[11\bar{2}]$ direction, which is consistent well with the experimental results. The angle φ can also be estimated as

$$\varphi = \arctan \frac{(n_{A\delta} + n_{B\delta} - n_{C\delta})|A\delta|}{2(n_{A\delta} + n_{B\delta} + n_{C\delta})d_{(111)}} = 6.7°, \tag{7}$$

where the ratio between $A\delta$, $B\delta$ and $C\delta$ ($n_{A\delta}$: $n_{B\delta}$: $n_{C\delta}$) is 1:1:1 for the ITB. Noteworthy, the ITB moves to the right about 0.6 nm along with the partial dislocation as shown by the experimental results. Possible reason is that the exchange reaction between the 1/3[111] partial and ITB dislocations

cause the migration of the ITB associated with the dislocation motion.

Medlin *et al.*[24] have reported the glide and climb of 1/3 partial dislocations on Σ3 twin boundaries in Al crystal. The glide of a/3[111] dislocations reportedly occurs along the Σ3 {112} incoherent twin boundary and introduces a slide of the ITB. The climb of a/3[111] dislocations take place along the Σ3 {111} coherent twin boundary and with an extent of tens of nanometers along the $[11\bar{2}]$ direction. This dislocation climb can thicken twin lamellae and cause a migration of ITB segments. In contrast to the present observations, the glide and climb of a/3[111] dislocations in Al take place independently on the (112) and (111) planes, respectively. Therefore, the dislocation moves either on the (112) plane and cause an ITB sliding or on the (111) plane and cause a migration of ITB segment. This is significantly different from the ITB migration with the moving of a/3[111] dislocations along a certain plane about 6.7° away from the (112) boundary plane as observed in the present work. The severe irradiation effect in their observation of aluminum and different stack fault energies between aluminum and copper may explain the different phenomena observed in the previous and present experiments. Molecular dynamics calculations suggest that the motion of ITBs can be accomplished by the glide of interface disconnections with Burgers vectors 2 a/3[111] and step height of a/6[11$\bar{2}$], i.e., interface-disconnection-glide (IDG) mechanism.[25] Nevertheless, we have not observed the interface disconnections in this experiment.

C. Shear stress needed for the dislocation exchange

Since reactions (1) and (4) are energetically unfavorable, shear stresses are needed to induce the dissociation of dislocations $D\delta$. This shear stress can be estimated according to the attractive force between two parallel straight dislocations that the shear stress is sufficient to dissociate one dislocation into two dislocations with a distance equal to core width of the initial dislocation. Although this theory is well developed,[31,34] we recapitulate here the essential formulae that will be needed for this paper. The radial force per unit length between two parallel dislocations is given by the formula[31]

$$F = \frac{G}{2\pi d}[(b_1 * \xi) \times (b_2 * \xi)]$$
$$+ \frac{G}{2\pi(1-\upsilon)d}[(b_1 \times \xi) * (b_2 \times \xi)], \tag{8}$$

where d is the distance between two dislocations, $G \approx 48$ GPa is the shear modulus of Cu crystal,[35] $\xi = AB$ is the dislocation line vector, $\nu = 0.343$ is the Poisson ratio of copper, and b_1 and b_2 are Burgers vectors of the two dislocations. Take an example of reaction (1): $D\delta \rightarrow A\delta + DA$, we assume that atoms in the core of $D\delta$ shuffle to simultaneously form $A\delta$ and DA under applied stress, which are then separated by a distance equal to the core width of $D\delta$, i.e., $a/\sqrt{3}$.[28] At the distance $d = a/\sqrt{3}$, the attractive force between $A\delta$ and DA per unit dislocation line length can be derived as $F = 3.5a/\sqrt{2}$ GPa from Eq. (8). The resolved

shear stress for driving DA away from $A\delta$ can be described by $\tau = F/DA = 3.5$ GPa. Atomic shuffling has been revealed by MD simulation in the process of dislocation emission from grain boundaries.[36] Following a similar procedure, the attractive force between BD^T and $A\delta$, BD^T and $C\delta$, $A\delta$, and $C\delta$ are calculated about $1.2a/\sqrt{2}$ GPa, $2.4a/\sqrt{2}$ GPa, $4.1a/\sqrt{6}$ GPa, respectively. Therefore, the shear stress required for the reaction (4) is about 4.1 GPa, which suggests that reaction (4) is the most difficult process among all the dislocation reactions and will decide the course of this dislocation exchange. These stresses are within the level of normal local stress concentration due to the applied shear stress. For example, MD simulations show that the shear stress near stacking faults in Cu could reach 3.5 GPa.[37] Therefore, under certain applied shear stress, the reactions described in Eqs. (1)–(6) are applicable. Repetition of the above dislocation reactions could enable 1/3[111] partial to move continuously on the ITB.

D. Dissociation of 1/3[111] partial at the junction between CTB and ITB

An isolated 1/3[111] partial on a twin boundary has been reported to relax into two different structures.[38] One variant has a compact dislocation structure, while the other relaxes by emitting a Shockley partial dislocation according to:

$$D\delta \rightarrow D\gamma + \gamma\delta, \qquad (9)$$

where $D\gamma$ is a 90° Shockley partial. However, in this work, the Burgers vector of the emitted dislocation is determined as a 30° Shockley partial γA, as shown in Figs. 8(a) and 8(b). This suggests a different dissociation process here. As we discussed previously, when the 1/3[111] partial exchanges position with the partial dislocation $C\delta$, the 1/3[111] partial $D\delta$ dissociates into a full dislocation BD^T and two partial dislocations according to Eq. (6). Nevertheless, when the dislocation $D\delta$ reaches the end of the ITB, the 1/3[111] partial $D\delta$ also has the possibility to dissociate into a full dislocation DA and a partial dislocation δA according to Eq. (1), which

is more energetically favorable than reaction Eq. (4). In this case, attributing to the absence of the twinning lattice above, the full dislocation DA then dissociates into two partial dislocations, $D\gamma$ and γA, respectively, i.e.

$$DA \rightarrow D\gamma + \gamma A, \qquad (10)$$

where γA glides upward on $(11\bar{1})$ plane as the emitted 30° Shockley partial.

E. Application to the motion of high angle grain boundaries

This dislocation exchange process could act as a coupling grain boundary sliding and migration mechanism in materials, particularly, for short segments of grain boundaries. High angle grain boundaries can be considered as a set of 1/6{112} Shockley partial dislocations on every close-packed plane.[39,40] Grain boundaries with different misorientation angles (θ) will then comprise sets of Shockley partials with different ratios between the 30° and 90° dislocations (Table I). For example, $\Sigma3$ {112} 70.5° grain boundary has a ratio of 2:1 between the 30° and 90° dislocations. This is consistent with the common knowledge that $\Sigma3$ {112} ITBs are represented as a set of Shockley partial dislocation on every {111} plane with a repeated sequence $A\delta$: $B\delta$: $C\delta$. Here, $A\delta$ and $B\delta$ are 30° mixed partial dislocations; $C\delta$ is a 90° pure edge partial dislocation, respectively. For $\Sigma43$ {353} 80.6° grain boundary, the ratio between the 30° and 90° dislocations (n_{30}: n_{90}) is 1:1. Accordingly, the grain boundary is comprised of Shockley partials with a repeating four-dislocation sequence, which includes two 30° partial dislocations ($A\delta$ and $B\delta$) and two 90° partial dislocations ($C\delta$) (i.e., in a sequence of ...$A\delta\,C\delta\,B\delta\,C\delta$...).

Based on the dislocation exchange mechanism described above, 1/3[111] partial dislocation can also move along these high angle grain boundaries and induce the sliding and migration of the grain boundaries. It should be noted that the 1/3[111] partial dislocation is slightly different at the right half crystal (R) from the left half (L) due to the slightly change on the orientation of the (111) plane across the GB (Fig. 9(a)). Assume a 1/3[111] partial of the right half crystal ($D\delta^R$) locating at $\Sigma43$ {353} 80.6° grain boundary, as shown
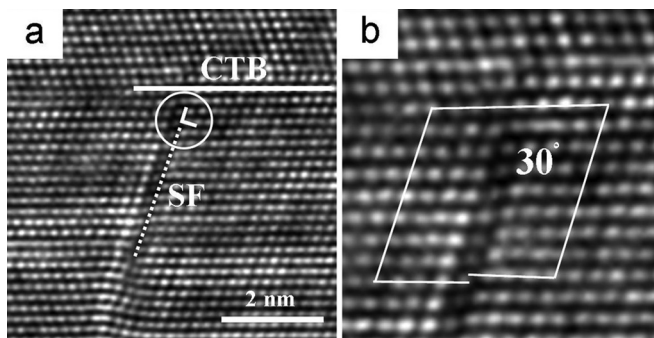

FIG. 8. (a) Schematics of the relation between $D\delta^R$ and $D\delta^L$. $D\delta^R$ is the 1/3[111] partial of the right half crystal (R); $D\delta^L$ is that of the left half crystal (L); (b) and (c) Schematics show the moving process of a 1/3[111] partial ($D\delta^R$) on the $\Sigma43$ {353} 80.6° grain boundary. The motion of the GB is indicated by black arrow. M and S are distances of grain boundary migration (indicated by blue arrow) and sliding (indicated by red arrow), respectively; The angle φ between ITB and the moving direction of the 1/3[111] dislocation is 5.1°. The viewing direction is [110].

TABLE I. Relationship between crystallographic parameters of high angle grain boundaries and GB sliding, migration components in fcc crystals.

GB	$\theta(°)$	n_{30}: n_{90}	$\varphi(°)$	S	M	β
$\Sigma = 11$	50.5	4:0	29.5	$-0.1\,l$	$0.57\,l$	-0.18
$\Sigma = 33$	59.0	6:1	20.0	$-0.036\,l$	$0.36\,l$	-0.1
$\Sigma = 3$	70.5	2:1	6.7	0	$0.12\,l$	0
$\Sigma = 43$	80.6	4:4	-5.1	$0.008\,l$	$-0.09\,l$	-0.09
$\Sigma = 17$	86.6	2:3	-4.1	$0.01\,l$	$-0.07\,l$	-0.14
$\Sigma = 17$	93.4	2:5	-2.8	$0.01\,l$	$-0.05\,l$	-0.02
$\Sigma = 43$	99.4	2:9	-1.7	$0.008\,l$	$-0.03\,l$	-0.27
$\Sigma = 3$	109.5	0:2	0	0	0	-

θ, tilt angle of GB; $n_{30}:n_{90}$, ratio between the 30° and 90° partial in the dislocation sequence; φ, angle between GB and the moving direction of the 1/3[111] dislocation; S and M, the distances of GB sliding and migration; β, coupling factor between the sliding and migration.
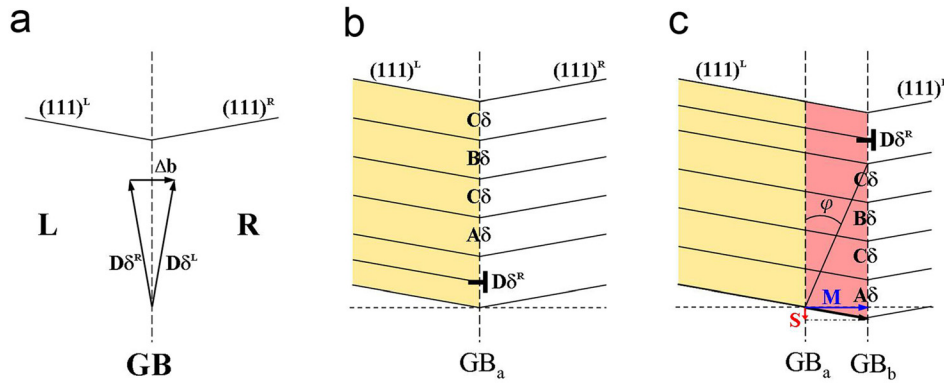
FIG. 9. (a) An HRTEM image of the emission of a Shockley partial (marked by the circle) from the location of 1/3[111] partial dislocation. (b) A Burgers circuit is drawn in the magnified image of the 30° Shockley partial in (a).

in Fig. 9(b). Driven by appropriate shear stress, the 1/3[111] partial dislocation will react, respectively, with grain boundary dislocations $A\delta$, $B\delta$ following Eqs. ((1)–(3)) and $C\delta$ following

$$D\delta^R \rightarrow C\delta + (A\delta + \Delta b) + BD^L, \tag{11}$$

$$BD^L + (A\delta + \Delta b) + C\delta \rightarrow D\delta^R. \tag{12}$$

After this process, the right half crystal will shift one (111) spacing up relative to the left half. Meanwhile, the GB will move along the direction within the $(111)^L$ plane (indicated by black arrow in Fig. 9(c)). This motion has a component

$$S = \tan\frac{\theta - \theta_0}{2}\tan\varphi * l, \tag{13}$$

along a direction within the GB plane (GB sliding) and the other component

$$M = \tan\varphi * l, \tag{14}$$

along the normal direction of the GB plane (GB migration) for a length l of the GB segment, as shown in Fig. 9(c). Here, θ is the tilt angle of the grain boundary, θ_0 is 70.53°, φ is the angle between GB and the moving direction of the 1/3[111] dislocation, which is determined by

$$\varphi = \arctan\frac{(n_{30°} - n_{90°})|A\delta|}{2(n_{30°} + n_{90°})d_{(111)}} - \frac{\theta - \theta_0}{2}. \tag{15}$$

For the $\Sigma43$ {353} 80.6° grain boundary, angle θ is 80.6°, and angle φ is $-5.1°$. Accordingly, the distances of GB sliding S and migration M are $0.008l$ and $0.09l$, respectively. For a typical GB segment of 20 nm, S and M will be 0.16 nm and 1.8 nm, respectively. The coupling factor between the sliding and migration $\beta = S/M$ is 0.09 in this case. For a general GB of {110} tilt axis, the coupling ratio is given by

$$\beta = \tan\frac{\theta - \theta_0}{2}. \tag{16}$$

Table I summarizes the distances of grain boundary sliding S and migration M for typical high angle grain boundaries with different misorientation angle.

V. CONCLUSIONS

The atomic structure of $\Sigma3$ {112} ITBs in nanotwinned Cu is investigated by using aberration-corrected high resolution transmission electron microscopy. It reveals that the dissociation width of the ITB is about two times of the {112} atomic spacing, which is considerably smaller than previous theoretical simulations.

By the use of *in situ* HRTEM, we have observed 1/3[111] Frank partial dislocation moving on the incoherent twin boundary in nanotwinned copper. This motion of 1/3[111] partial dislocation is accompanied by a migration of the ITB. A dislocation exchange model is proposed for the motion of 1/3[111] partial that the 1/3[111] partial exchanges its position with ITB partial dislocations in sequence. Theoretical calculation estimates the required shear stresses being not more than 4.1 GPa for the dislocation exchange reactions, which is at the reasonable level of local stress concentration during normal deformation. A move of the 1/3[111] partial along the direction normal to the ITB plane as well as the ITB migration are determined from *in situ* observation, and the movement is consistent with the proposed dislocation exchange mechanism. The present results present implications that the reaction between the 1/3[111] partial and ITB dislocations might cause the migration of the ITB associated with the dislocation motion.

[1]K. Lu, L. Lu, and S. Suresh, Science **324**, 349 (2009).
[2]Y. T. Zhu, X. Z. Liao, S. G. Srinivasan, and E. J. Lavernia, J. Appl. Phys. **98**, 034319 (2005).
[3]X. Y. Li, Y. J. Wei, L. Lu, K. Lu, and H. J. Gao, Nature **464**, 877 (2010).

[4]Y. M. Wang, F. Sansoz, T. LaGrange, R. T. Ott, J. Marian, T. W. Barbee, and A. V. Hamza, Nature Mater. **12**, 697 (2013).

[5]T. Zhu, J. Li, A. Samanta, H. G. Kim, and S. Suresh, Proc. Natl. Acad. Sci. U. S. A. **104**, 3031 (2007).

[6]E. A. Marquis, D. L. Medlin, and F. Léonard, Acta Mater. **55**, 5917 (2007).

[7]U. Wolf, F. Ernst, T. Muschik, M. W. Finnis, and H. F. Fischmeister, Philos. Mag. A **66**, 991 (1992).

[8]F. Ernst, M. W. Finnis, A. Koch, C. Schmidt, B. Straumal, and W. Gust, Z. Metall. **87**, 911 (1996).

[9]G. H. Campbell, D. K. Chan, D. L. Medlin, J. E. Angelo, and C. B. Carter, Scr. Mater. **35**, 837 (1996).

[10]J. D. Rittner and D. N. Seidman, Phys. Rev. B **54**, 6999 (1996).

[11]J. D. Rittner, D. N. Seidman, and K. L. Merkle, Phys. Rev. B **53**, R4241 (1996).

[12]C. Schmidt, M. W. Finnis, F. Ernst, and V. Vitek, Philos. Mag. A **77**, 1161 (1998).

[13]M. A. Tschopp and D. L. McDowell, Philos. Mag. **87**, 3147 (2007).

[14]V. Randle, Acta Mater. **47**, 4187 (1999).

[15]Y. B. Wang and M. L. Sui, Appl. Phys. Lett. **94**, 021909 (2009).

[16]Z. H. Jin, P. Gumbsch, K. Albe, E. Ma, K. Lu, H. Gleiter, and H. Hahn, Acta Mater. **56**, 1126 (2008).

[17]D. P. Field, R. C. Eames, and T. M. Lillo, Scr. Mater. **54**, 983 (2006).

[18]D. P. Field, B. W. True, T. M. Lillo, and J. E. Flinn, Mater. Sci. Eng. A **372**, 173 (2004).

[19]J. Wang, N. Li, O. Anderoglu, X. Zhang, A. Misra, J. Y. Huang, and J. P. Hirth, Acta Mater. **58**, 2262 (2010).

[20]J. Wang, O. Anderoglu, J. P. Hirth, A. Misra, and X. Zhang, Appl. Phys. Lett. **95**, 021908 (2009).

[21]L. Liu, J. Wang, S. K. Gong, and S. X. Mao, Phys. Rev. Lett. **106**, 175504 (2011).

[22]L. Xu, D. Xu, K. N. Tu, Y. Cai, N. Wang, P. Dixit, J. H. L. Pang, and J. Miao, J. Appl. Phys. **104**, 113717 (2008).

[23]J. A. Brown and N. M. Ghoniem, Acta Mater. **57**, 4454 (2009).

[24]D. L. Medlin, C. B. Carter, J. E. Angelo, and M. J. Mills, Philos. Mag. A **75**, 733 (1997).

[25]J. Wang, A. Misra, and J. P. Hirth, Phys. Rev. B **83**, 064106 (2011).

[26]L. Lu, Y. F. Shen, X. H. Chen, L. H. Qian, and K. Lu, Science **304**, 422 (2004).

[27]L. Lu, T. Zhu, Y. F. Shen, M. Dao, K. Lu, and S. Suresh, Acta Mater. **57**, 5165 (2009).

[28]See supplementary material at http://dx.doi.org/10.1063/1.4861868 for sample preparation, a periodic pattern of contrast in HRTEM images of ITBs, the change of lattice orientations, the location of ITBs, the critical distance between two dislocations and dynamic process of the 1/3[111] partial moving on the ITB.

[29]K. Du, F. Ernst, M. C. Pelsozy, J. Barthel, and K. Tillmann, Acta Mater. **58**, 836 (2010).

[30]K. Du, Y. Rau, N. Y. Jin-Phillipp, and F. Phillipp, J. Mater. Sci. Technol. **18**, 135 (2002).

[31]J. P. Hirth and J. Lothe, *Theory of Dislocations* (McGraw-Hill, 1968).

[32]Y. T. Zhu, X. L. Wu, X. Z. Liao, J. Narayan, L. J. Kecskés, and S. N. Mathaudhu, Acta Mater. **59**, 812 (2011).

[33]A. H. Zewail and J. M. Thomas, *4D Electron Microscopy* (Imperial College Press, London, 2010).

[34]Y. T. Zhu, X. L. Wu, X. Z. Liao, J. Narayan, S. N. Mathaudhu, and L. J. Kecskes, Appl. Phys. Lett. **95**, 031909 (2009).

[35]M. A. Meyers and K. K. Chawla, *Mechanical Behavior of Materials* (Cambridge University Press, 2009).

[36]H. Van Swygenhoven, P. M. Derlet, and A. G. Froseth, Nat. Mater. **3**, 399 (2004).

[37]J. Wang and H. Huang, Appl. Phys. Lett. **85**, 5983 (2004).

[38]E. A. Marquis and D. L. Medlin, Philos. Mag. Lett. **85**, 387 (2005).

[39]G. Lucadamo and D. L. Medlin, Science **300**, 1272 (2003).

[40]D. L. Medlin, S. M. Foiles, and D. Cohen, Acta Mater. **49**, 3689 (2001).